Available online at www.sciencedirect.com
SCIENCE DIRECT®
Journal of Chromatography A, 1079 (2005) 105–115
JOURNAL OF CHROMATOGRAPHY A
www.elsevier.com/locate/chroma

Two-component protein adsorption kinetics in porous ion exchange media

Cristina Martin, Gunter Iberer[1], Antonio Ubiera, Giorgio Carta*

Department of Chemical Engineering, University of Virginia, Charlottesville, VA 22904-4741, USA

Available online 19 March 2005

Abstract

This work provides a theoretical analysis of multicomponent adsorption kinetics for conditions typical of protein adsorption in porous ion exchangers as well as experimental results for the adsorption of lysozyme/cytochrome *c* mixtures in the cation exchanger SP-Sepharose-FF. The theory predicts the formation of overshoots in the intraparticle concentration profiles and in the total amount adsorbed for the more weakly adsorbed component. An analytical solution valid for the case where the isotherms are rectangular is developed and found to be in good agreement with the limiting behavior of the general numerical solution of the model equations. The experimental results show that the two proteins are competitively adsorbed and that an overshoot of adsorbed cytochrome *c* occurs during simultaneous adsorption. Model predictions based on the assumption that the adsorption isotherms are rectangular and that lysozyme completely displaces cytochrome *c* are in qualitative and quantitative agreement with the experimental kinetics suggesting that the overshoot phenomena observed with multicomponent systems in these resins can be explained with a diffusion model without the need to account for flux coupling or electrophoretic contributions to transport.

Keywords: Protein adsorption kinetics; Ion exchange; Mass transfer modeling

1. Introduction

Rational design of protein ion exchange chromatography processes requires an understanding of the rate at which the proteins bind to the ion exchange sites. When using media suitable for process scale applications, this rate is typically controlled by diffusion within the particles. Thus, an understanding of diffusion rates is critical. Although many authors have investigated single protein ion exchange rates, very few have considered the case of multicomponent competitive protein adsorption systems. In an early study, Skidmore and Chase [1] investigated the simultaneous adsorption of lysozyme and bovine serum albumin (BSA) in columns packed with the cation exchanger SP-Sepharose-FF. Adsorption of the two proteins was shown to be competitive but the kinetics of the binding process was not determined. In another study, Weinbrenner and Etzel [2] investigated the simultaneous adsorption of BSA and lactalbumin on cation exchange membranes. These authors reached the same conclusion with regards to the competitive nature of protein binding leading to a "roll up" of the less strongly adsorbed protein under near local equilibrium conditions.

Lewus and Carta [3] investigated the kinetics of two-component protein adsorption on the cation exchanger S HyperD-M for mixtures of cytochrome *c* and lysozyme. S HyperD-M comprises porous silica particles whose pores are filled with a charged poly(acrylamide) gel. The observed adsorption kinetics was found to be consistent with diffusional transport through a tight fitting charged gel mesh. Thus, single and two-component mass transfer rates were described in terms of a homogeneous diffusion model, where the driving force for diffusion is given by the adsorbed protein concentration gradient. Accordingly, the ensuing intraparticle concentration profiles were predicted to be smooth. Based on microscopic visualization studies with capillary supported gels, the existence of such smooth profiles consistent with a homogeneous diffusion model was later confirmed experimentally for both single and multicomponent systems [4–7].

* Corresponding author. Tel.: +1 434 924 6281; fax: +1 434 982 2658.
E-mail address: gc@virginia.edu (G. Carta).
[1] Present address: Octapharma Inc., Vienna, Austria.

0021-9673/$ – see front matter © 2005 Elsevier B.V. All rights reserved.
doi:10.1016/j.chroma.2005.03.007

The kinetics of adsorption of fluorescently labeled proteins in SP-Sepharose-FF particles has been studied by means of confocal microscopy by several authors [8–11]. SP-Sepharose-FF is based on a crosslinked, functionalized agarose matrix with relatively large pores [12]. Crosslinked agarose is thought to form a rigid pore structure. As a result, transport in this matrix is likely to occur principally by diffusion through the liquid-filled pores. Since the pores are large compared to the size of typical proteins, diffusional transport is likely unaffected by electrostatic interactions with the pore wall. In this case, the intraparticle concentration profiles tend to be sharp when the binding isotherm is favorable. This behavior has been confirmed experimentally at low ionic strengths based on confocal microscopy studies [9–11]. However, departures from this behavior have also been noted at higher ionic strengths, sometime accompanied by sharp, temporary overshoots in fluorescence intensity [10,11]. Various explanations have been advanced for this behavior as discussed by Hubbuch et al. [13]. Nonetheless, the hypothesis of sharp profiles appears to hold, at least at low ionic strengths.

A theoretical study of two-component protein adsorption in spherical ion exchange particles has been reported recently by Gallant [14] based on the numerical solution of a pore diffusion model. In this work, protein adsorption equilibrium was described by the steric mass action model (SMA) [15]. Accordingly, displacement of salt counterions from the resin was assumed to occur during protein adsorption as required to maintain electroneutrality in the adsorbed phase. As a result, a salt concentration gradient was predicted inside the particle. The magnitude of the induced salt gradient is, however, generally very small, since, in practice, even in dilute buffer solutions, the salt concentration is much greater than the equivalent protein concentration. For example, in Gallant's reported detailed calculations, the maximum excursion in salt concentration from the initial value within the particles was only about 0.4%, suggesting that the assumption of a constant salt concentration is probably valid in most practical cases.

The present work has two components. The first is the development of a general pore-diffusion model to describe two-component protein binding with emphasis on the theoretical description of intraparticle concentration profiles along with the derivation of limiting analytical solutions valid for the case of a rectangular isotherm. The second is an experimental investigation of the kinetics of two-component protein adsorption in SP-Sepharose-FF. For this investigation we use mixtures of cytochrome *c* and lysozyme, which can be detected spectrophotometrically. Both simultaneous and sequential adsorption are considered. In the first case, the two proteins co-diffuse in the particles, while in the second the two proteins diffuse in opposite direction. Batch and shallow-bed experimental results are obtained for each pure component and various mixtures of the two and compared with the theoretical development.

2. Theoretical development

We consider the competitive adsorption of two components assuming that intraparticle mass transfer occurs by diffusion in liquid-filled pores with a driving force expressed in terms of the pore fluid concentration gradient. The following four assumptions are made: (1) the adsorbent particles are spherical and chemically and structurally homogeneous; (2) the pore fluid concentration is locally in equilibrium with the adsorbed phase concentration; (3) the pore fluid concentration is much smaller than the adsorbed-phase concentration; and (4) the adsorption equilibrium is represented by the multicomponent Langmuir isotherm according to:

$$q_i = \frac{q_{\mathrm{m},i} K_i C_i}{1 + \sum K_j C_j} \tag{1}$$

The following conservation equations and boundary conditions can be written to describe adsorption in a finite-bath batch adsorption system:

$$\frac{\partial q_i}{\partial t} = \frac{D_{\mathrm{e},i}}{r^2} \frac{\partial}{\partial r} \left(r^2 \frac{\partial c_i}{\partial r} \right) \tag{2}$$

$$t = 0: \quad c_i = 0, \qquad q_i = 0 \tag{2a}$$

$$r = 0: \quad \frac{\partial c_i}{\partial r} = 0 \tag{2b}$$

$$r = r_\mathrm{p}: \quad D_{\mathrm{e},i} \frac{\partial c_i}{\partial r} = k_{\mathrm{f},i}(C_i - C_i^\mathrm{s}) \tag{2c}$$

$$\frac{\mathrm{d}C_i}{\mathrm{d}t} = \frac{3k_{\mathrm{f},i}}{r_\mathrm{p}} \frac{V_\mathrm{M}}{V}(C_i - C_i^\mathrm{s}) = -\frac{V_\mathrm{M}}{V} \frac{\mathrm{d}\bar{q}_i}{\mathrm{d}t} \tag{3}$$

$$t = 0: \quad C_i = C_i^0 \tag{3a}$$

In these equations, q_i is the adsorbed concentration of component i, c_i and C_i are the pore fluid and external solution concentrations, respectively, $D_{\mathrm{e},i}$ is the effective pore diffusivity, $k_{\mathrm{f},i}$ the external mass transfer coefficient, V_M the volume of the particles, V the volume of solution, and $\bar{q}_i$ is the adsorbed concentration averaged over the particle volume.

Since the isotherm is nonlinear, a numerical solution of Eqs. (1)–(3) is required in general and was obtained by finite differences. On the other hand, analytical solutions can also be found for certain limiting cases. The first is the Henry's law limit of the isotherm. Here, however, the results are trivial since adsorption of the two species would occur independently. A second, more interesting case, is the irreversible isotherm limit, which occurs when

$$R_i = \frac{1}{1 + K_i C_i} \ll 1 \tag{4}$$

In this case, the adsorbent is nearly completely saturated. Thus, for each pure component, at equilibrium $q_i^* \approx q_{\mathrm{m},i}$. When both components are present, the relative amounts of

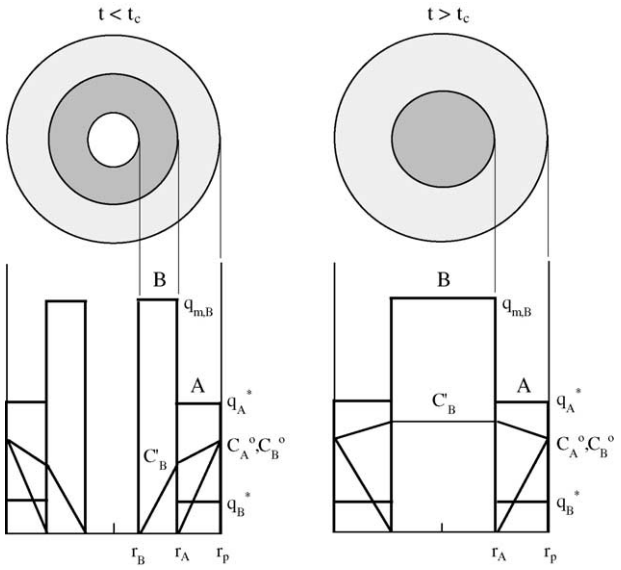

Fig. 1. Sketch of intraparticle concentration profiles for the case of rectangular isotherms with A displacing B.

each adsorbed species are related by

$$\frac{q_A^*}{q_B^*} = \frac{q_{m,A}K_A}{q_{m,B}K_B}\frac{C_A}{C_B} \tag{5}$$

Here simultaneous adsorption of the two components occurs in two regimes as shown in Fig. 1 for the case where A displaces B. For a time $t < t_c$ there are two adsorption fronts. In the outermost layer ($r_A < r < r_p$), both A and B are present in the pores while in the middle layer ($r_B < r < r_A$), only B is present. In the latter layer $q_A = 0$ and $q_B = q_{m,B}$. Finally, in the central core ($r < r_B$), there is neither A nor B. For $t > t_c$, the inner core has completely disappeared as the adsorptive front of B has reached the center of the particle. In this case, there is a single adsorption front for A.

The approach followed in this development is similar to the analysis of Arevalo et al. [16], although there are a few significant differences that will be pointed out later. For simplicity, in deriving the analytical solution we make the additional assumption that the external mass transfer resistance is negligible and that adsorption takes places in an infinite volume bath. The derivation is then straightforward for each regime assuming a pseudo steady state as in the classical shrinking core model for single component adsorption [17].

2.1. Solution for $t < t_c$

With reference to Fig. 1, in the outermost layer ($r_A < r < r_p$), we have:

$$r^2 D_{e,A}\frac{dc_A}{dr} = k_A \tag{6}$$

$$r^2 D_{e,B}\frac{dc_B}{dr} = k_B \tag{7}$$

$$r = r_p: \quad c_A = C_A, \qquad c_B = C_B \tag{8a}$$

$$r = r_A: \quad c_A = 0, \qquad c_B = c'_B \tag{8b}$$

Eqs. (6) and (7) are the same as those used by Arevalo et al. However, the boundary condition expressed by Eq. (8b) is different. Arevalo et al. assumed $c_B(r_A) = C_B$, but this is inconsistent since a concentration gradient of B must exist through the outermost layer also. Integrating Eqs. (6) and (7) we obtain

$$k_A = \frac{D_{e,A}C_A}{(1/r_A) - (1/r_p)} \tag{9}$$

$$k_B = \frac{D_{e,B}(C_B - c'_B)}{(1/r_A) - (1/r_p)} \tag{10}$$

The advancement of the adsorption front for A is obtained from the balance equation

$$q_A^* r_A^2 \frac{dr_A}{dt} = \frac{D_{e,A}C_A}{(1/r_p) - (1/r_A)} \tag{11}$$

$$t = 0: \quad r_A = r_p \tag{11a}$$

Integrating this equation and introducing dimensionless variables we obtain the result

$$2\rho_A^3 - 3\rho_A^2 + 1 = \frac{t}{\tau_A} \tag{12}$$

where $\rho_A = r_A/r_p$ and $\tau_A = q_A^* r_p^2/6D_{e,A}C_A$. The latter represents the time needed for A to completely saturate the particle. This result is the same as that obtained for adsorption of a single component [17].

In the middle layer ($r_B < r < r_A$), we have

$$r^2 D_{e,B}\frac{dc_B}{dr} = k'_B \tag{13}$$

$$r = r_A: \quad c_B = c'_B \tag{13a}$$

$$r = r_B: \quad c_B = 0 \tag{13b}$$

Integrating this equation we obtain

$$k'_B = \frac{D_{e,B}c'_B}{(1/r_B) - (1/r_A)} \tag{14}$$

As before, the advancement of the adsorption front for B is obtained from the following balance and boundary condition

$$q_{m,B} r_B^2 \frac{dr_B}{dt} = \frac{D_{e,B}c'_B}{(1/r_A) - (1/r_B)} \tag{15}$$

$$t = 0: \quad r_B = r_p \tag{15a}$$

However, before this equation can be integrated, we must find c'_B, the concentration at the interface between the two layers. This is found by considering that when an amount q_A^* of A is adsorbed at the adsorption front, an amount $q_{m,B} - q_B^*$ of B is displaced. The corresponding flux of B is thus divided in two parts: a flux toward the center of the particle and one

toward the outside. A material balance at the A adsorption front gives

$$\frac{q_{m,B}-q_B^*}{q_{m,A}}\frac{D_{e,A}C_A}{(1/r_A)-(1/r_p)} = \frac{D_{e,B}c'_B}{(1/r_B)-(1/r_A)} + \frac{D_{e,B}(c'_B-C_B)}{(1/r_A)-(1/r_p)} \quad (16)$$

which can be solved for c'_B yielding the following dimensionless result:

$$\frac{c'_B}{C_B} = \frac{1+(1/\beta)}{1+[(1-(1/\rho_A))/((1/\rho_A)-(1/\rho_B))]} \quad (17)$$

where $\rho_B = r_B/r_p$ and $\beta = q_A^* D_{e,B} C_B/(q_{m,B}-q_B^*)D_{e,A}C_A$. The final result for the adsorption front of B is found by substituting Eq. (17) in Eq. (15) and integrating yielding

$$2\rho_B^3 - 3\rho_B^2 + 1 = (1+\beta)\frac{q_{m,B}-q_B^*}{q_{m,B}}\frac{t}{\tau_A} \quad (18)$$

One can see that the B adsorption front reaches the center of the particle when

$$t = t_c = \frac{q_{m,B}}{q_{m,B}-q_B^*}\frac{\tau_A}{1+\beta} \quad (19)$$

2.2. Solution for $t > t_c$

In this regime there is only one adsorption front, while the central core is completely saturated with B. The position of the A front is still given by Eq. (12). However, for B, from Eq. (17) we obtain

$$\frac{c'_B}{C_B} = 1 + \frac{1}{\beta} \quad (20)$$

In this case, B is continually desorbed until $\rho_A = 0$.

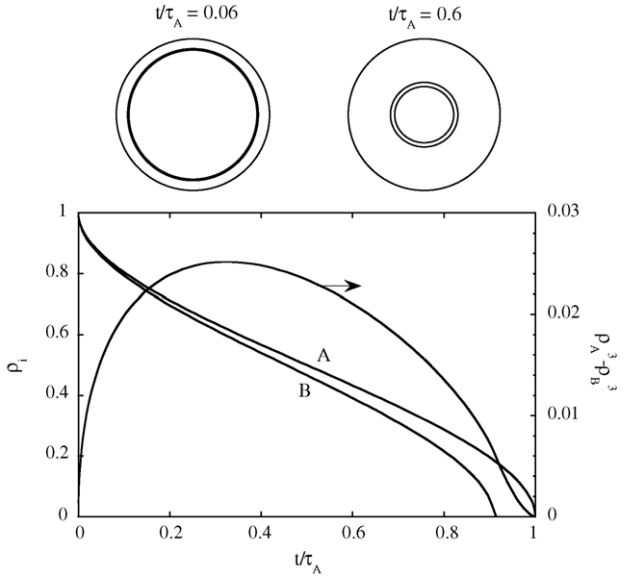

Fig. 2. Dimensionless position of adsorption fronts for $\beta = 0.1$.

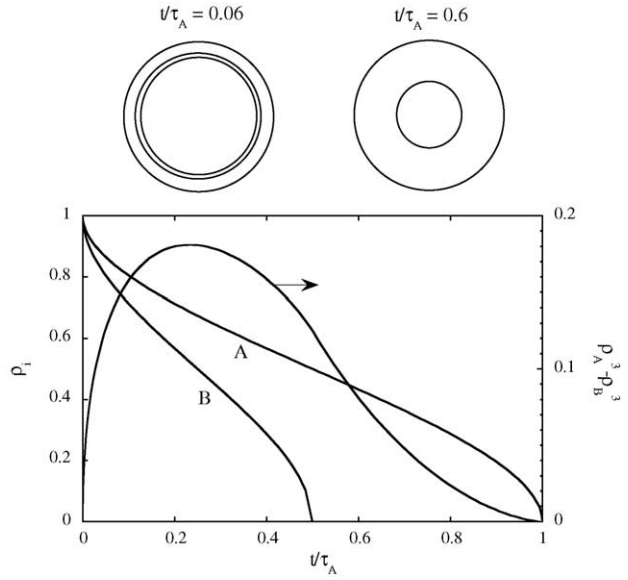

Fig. 3. Dimensionless position of adsorption fronts for $\beta = 1$.

The behavior of the analytical solution is shown in Figs. 2 and 3 for different values of β. The graphs shows the dimensionless position of the two adsorption fronts as a function of time as well as the quantity $\rho_A^3 - \rho_B^3$, which represents the temporary overshoot of B above the equilibrium value. It can be seen that smaller values of β result in a thinner middle layer for $t < t_c$ and a smaller B-core for $t > t_c$.

The above analytical solution is extended to the case of N components in Appendix A and to the case of adsorption from a finite bath including the external mass transfer resistance in Appendix B.

3. Computational results

Numerical calculations were performed for three representative cases as summarized in Table 1. For all three cases we assume an infinite volume bath and neglect the external resistance. In the first (Case I), we have chosen $C_A \gg C_B$ along with Langmuir equilibrium constants that are similar to each other. In addition, we have chosen conditions so that $R_A \ll 1$. These conditions are representative of favorable adsorption of a bulk component along with a minor, closely related

Table 1
Conditions for numerical simulations of two-component adsorption in an infinite bath

	Case I	Case II	Case III
C_A (mg/cm^3)	1	1	1
C_B (mg/cm^3)	0.01	1	1
K_A (cm^3/mg)	100	1	1000
K_B (cm^3/mg)	90	0.01	10

$q_{m,A} = q_{m,B} = 235$ mg/cm^3, $D_{e,A} = D_{e,B} = 2.2 \times 10^{-7}$ cm^2/s, $r_p = 0.005$ cm.

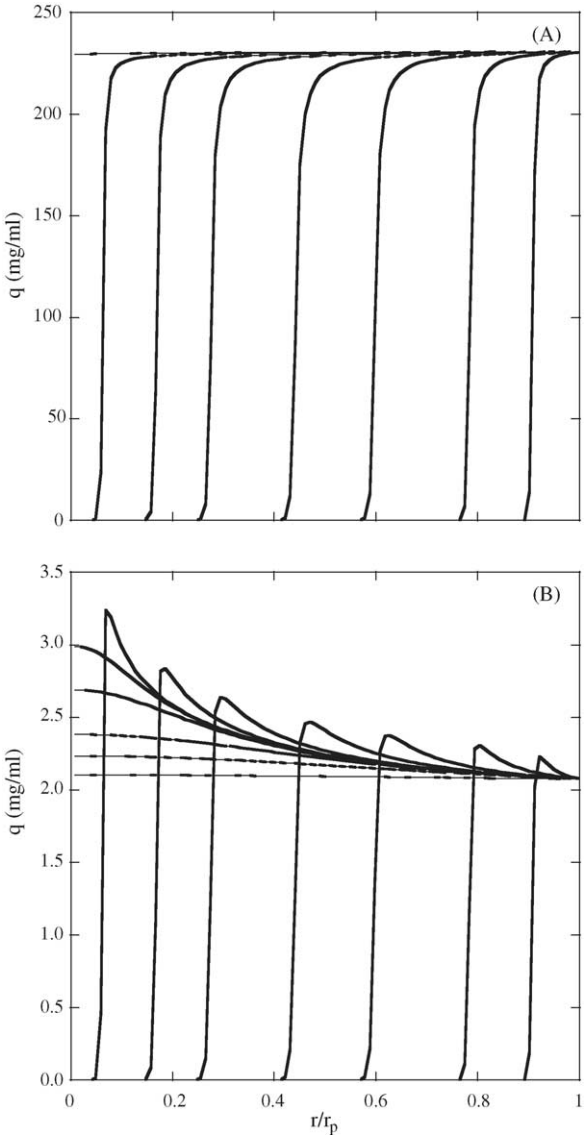

Fig. 4. Concentration profiles for Case I shown at $t = 100$, 500, 1500, 2500, 3500, 4000, 4300, 4400, 4500, 4600, 6000, and 10,000 s.

impurity. For this case, the isotherms are approximated by

$$q_A \approx \frac{q_{m,A} K_A C_A}{1 + K_A C_A} \approx q_{m,A}$$

$$q_B \approx \frac{q_{m,B} K_B}{1 + K_A C_A} C_B$$

Note that here the B isotherm is approximately linear when C_A is finite while the A isotherm is rectangular. The evolution of intraparticle concentration profiles and the average adsorbed concentrations for this case are shown in Figs. 4 and 5, respectively. Since A is in large excess, the amount of A adsorbed at equilibrium is much higher than that of B. Accordingly, B accumulates ahead of the A adsorption front resulting in an overshoot above the equilibrium concentration. The overshoot moves inwardly and for longer times is transformed into a B-saturated core. From

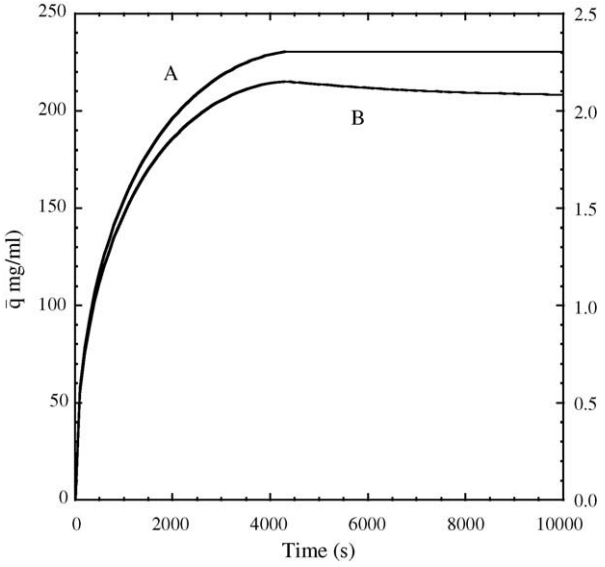

Fig. 5. Average concentrations in particle for Case I.

this point on desorption of B occurs as the system gradually approaches equilibrium. As seen in Fig. 5, an overshoot is also predicted for the particle-average concentration, $\bar{q}_B$, although this overshoot is much less noticeable than that in the intraparticle profiles. The A intraparticle profiles propagate with a sharp front barely distinguishable from that predicted by the classical single component shrinking core model.

For the second case in Table 1 (Case II), we have chosen $C_A = C_B$, but very different Langmuir constants, with component A much more strongly adsorbed than B ($K_A \gg K_B$) and $R_A \sim 1$. These conditions correspond to the adsorption of two fairly different components with a moderately favorable competitive isotherm. As in the previous case, the adsorbed equilibrium concentration of B is much lower than that of A. Calculated intraparticle concentration profiles and the particle average concentrations for this case are shown in Figs. 6 and 7. As before, the B profile exhibits an overshoot above equilibrium. However, since the fluid phase concentration of B is much higher than in Case I, B diffuses faster in the particle approaching the center for much shorter times. Correspondingly, the overshoot in the average B concentration occurs for very short times followed by a gradual return to equilibrium conditions when the particle becomes saturated with A. Unlike Case I, the A profiles are smooth owing to the reversible nature of the isotherm.

Finally, for the third case in Table 1 (Case III) we have chosen a situation where again $C_A = C_B$ and $K_A \gg K_B$, but both R_A and R_B are much less than one. In this case, we have two strongly bound components with nearly rectangular isotherms but with A nearly completely displacing B. These conditions are thus similar to the ones invoked in the derivation of the limiting analytical solution. Calculated intraparticle profiles and particle average concentrations for this case are shown in Figs. 8 and 9. As in Case II, component B diffuses faster than A in the particle accumulating ahead of the

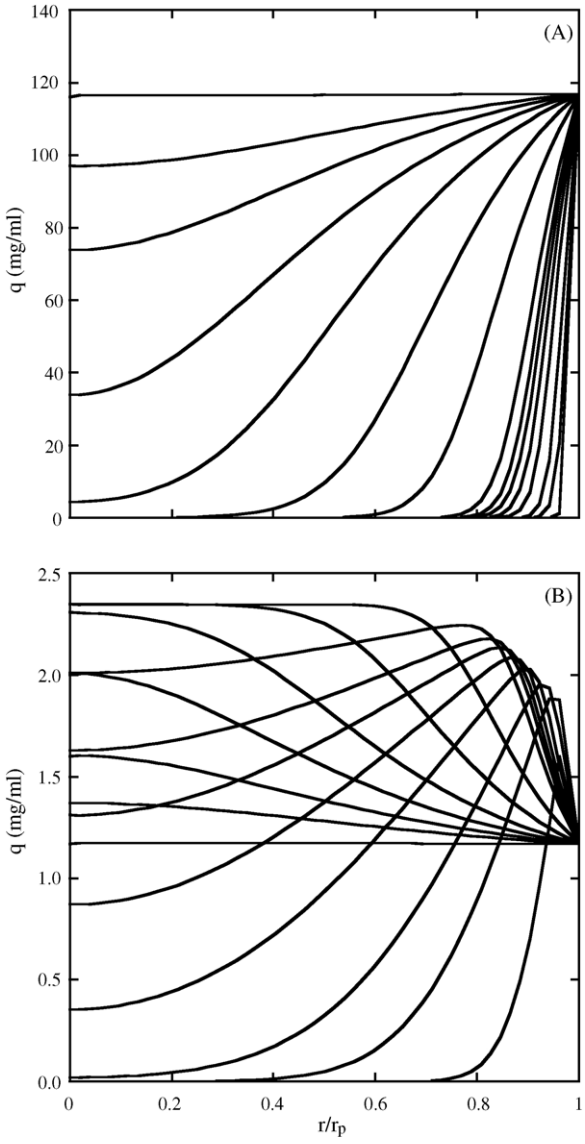

Fig. 6. Concentration profiles for Case II shown at $t = 1$, 5, 10, 20, 30, 40, 50, 70, 200, 500, 1000, 1500, 2000, 2500, 5000 s.

A-front. Desorption of B ensues when the B-front reaches the center of the particle until equilibrium is established with an almost zero adsorbed concentration of B. Both the A and B profiles are sharp. The analytical result (Eqs. (12) and (18)) is also shown in Fig. 9. For these conditions we see that there is excellent agreement between the limiting analytical solution and the numerical results. The former can thus be used with good accuracy even if the predicted concentration profiles are not perfectly sharp.

4. Experimental studies

The goal of the experimental work was to determine the actual kinetics of two-component protein adsorption systems and compare the results with the theoretical analyses.

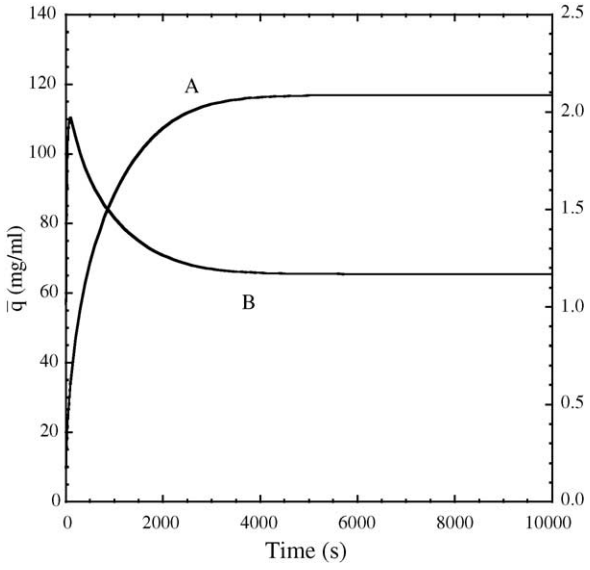

Fig. 7. Average concentrations in particle for Case II.

4.1. Materials and methods

The adsorbent used in this work is SP-Sepharose-FF (Amerhsam Biosciences, Uppsala, Sweden). This material is an agarose-based sulfopropyl cation exchanger with a particle diameter of approximately 100 μm for the lot used in this work [18]. Chicken egg white lysozyme ($M_r = 14{,}500$, p$I = 11$) and cytochrome *c* from bovine heart ($M_r = 12{,}500$, p$I = 10.6$) from Sigma Chemical Company (St. Louis, MO, USA) were used as model proteins. All other chemicals were obtained from Sigma or Fisher Scientific (Pittsburgh, PA). All experiments were performed at room temperature ($23 \pm 2\,^{\circ}C$) in 10 mM Na_2HPO_4 aqueous buffer at pH 6.5. At this pH, both lysozyme and cytochrome *c* are positively charged.

Single component equilibrium isotherms were obtained by contacting small samples of media (0.025 cm^3 wet settled media) with 10 cm^3 samples of protein solutions of known initial concentration and determining the residual solution concentrations at equilibrium. Amounts adsorbed were then calculated from material balances. Adsorption was reversible as virtually complete recovery of the bound protein could be obtained in buffer solutions containing 1 M sodium chloride.

Single and two-component adsorption kinetics were obtained using both stirred-batch and shallow-bed methods. Stirred batch experiments were done by suspending 0.1–0.3 cm^3 of hydrated particles in a 100 cm^3 protein solution agitated with a magnetic stirrer while continuously monitoring the protein concentration in solution. The apparatus is the same as that described in ref. [19] except that two UV–vis detectors (Amersham Biosciences, Mod. UV-1) were used in series to allow detection at 405 and 280 nm. Since lysozyme has no absorbance at 405 nm, individual protein concentrations were obtained by determining the cytochrome *c* concentration at 405 nm and subtracting its contribution to the total absorbance at 280 nm to determine the lysozyme

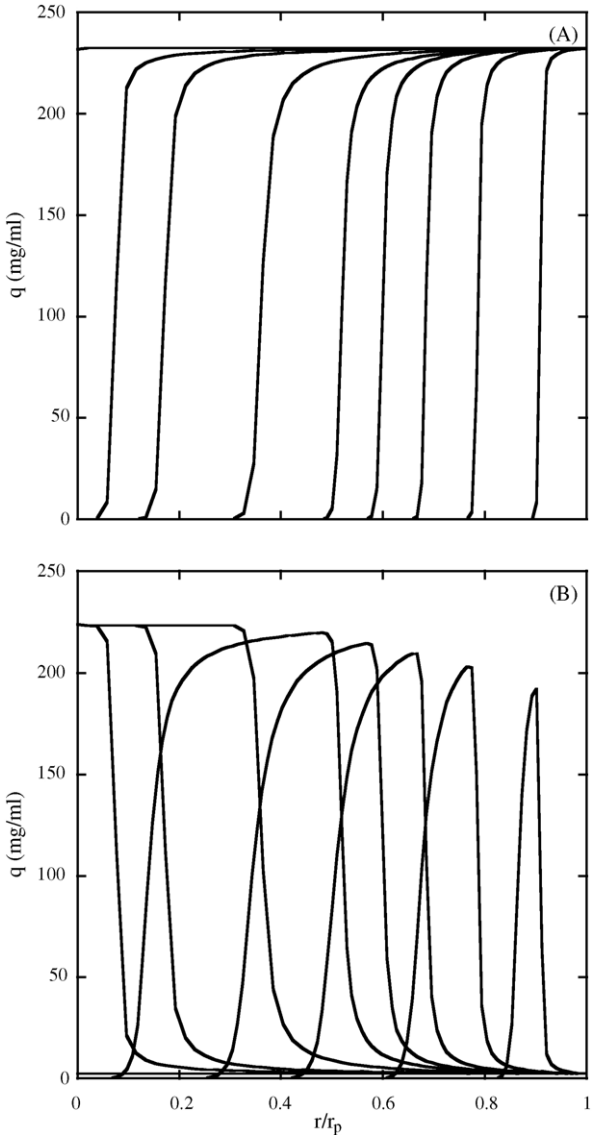

Fig. 8. Concentration profiles for Case III shown at t = 100, 500, 1000, 1500, 2000, 3000, 4000, 4300, 5000 s.

concentration as discussed in ref. [20]. Experiments were done for both simultaneous and sequential adsorption, in the first case starting with clean adsorbent samples and in the second starting with a pre-saturated adsorbent sample.

Shallow-bed experiments were conducted in a manner similar to that described in ref. [18]. For these experiments, a small sample of SP-Sepharose-FF (∼5 μL) was placed in a 0.5-cm ID glass chromatographic column fitted with two adjustable plungers (Amersham Biosciences, Model HR 5/5). For an uptake experiment, a protein solution is passed through this column for a certain period of time at a high flow rate (4 cm^3/min). Excess protein is then quickly removed from the extraparticle voids by feeding the protein-free buffer and the amount of bound protein determined by desorption with 500 mM NaCl. The area of the desorption peak is related to the amount of protein bound. The column is then

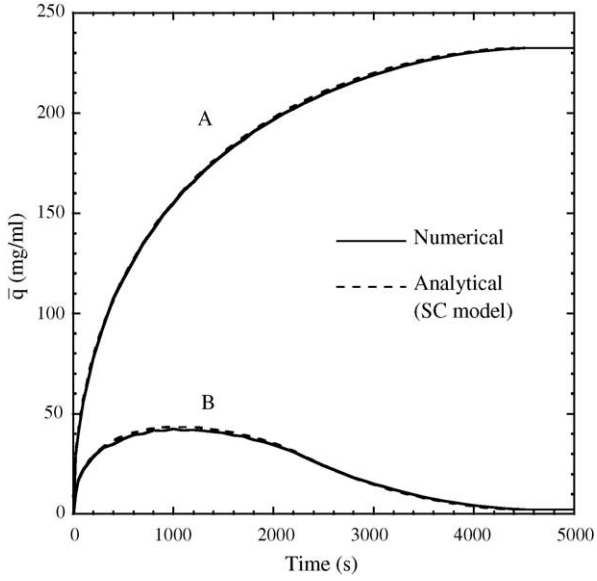

Fig. 9. Average concentration profiles for Case III. The numerical and analytical solutions are nearly coincident.

reequilibrated in buffer and the cycle repeated for a different adsorption time. As in the batch experiments, the amounts of each protein adsorbed were determined by combining the 405 and 280 nm detector signals. Since the amount of adsorbent is very small and the mobile phase velocity is very high, adsorption occurs under essentially constant protein concentration in solution, or for conditions approximating an infinite bath. An AKTA Explorer liquid chromatography system (Amersham Biosciences) was used for these experiments.

4.2. Experimental results

Single component isotherms are shown in Fig. 10. The lines are fits with the Langmuir model although the isotherms can obviously be approximated as being nearly rectangular with capacities of 230 ± 20 and 130 ± 10 mg/cm^3 for lysozyme and cytochrome *c*, respectively. The substantial difference in capacity is surprising. However, there are 11 arginines and 6 lysines in lysozyme while there are only 2 arginines and 16 lysines in cytochrome *c*. Thus, it is possible that the stronger binding of lysozyme occurs because the positive charges in lysozyme are mostly associated with the substantially more basic arginine residues.

Single component batch uptake curves are shown in Fig. 11. These graphs show the amount adsorbed as a function of time, obtained from material balances. Good fits of the batch uptake curves were obtained with effective pore diffusivity values of 2.5×10^{-7} and 2.0×10^{-6} cm^2/s, respectively, using a film mass transfer coefficient k_f = 0.003 cm/s. The latter was determined in prior work [3], but had an almost negligible effect on the calculated curves. Since the isotherms are very favorable, calculation based on the numerical solution of the pore diffusion model equations (Eqs. (1)–(3)) and

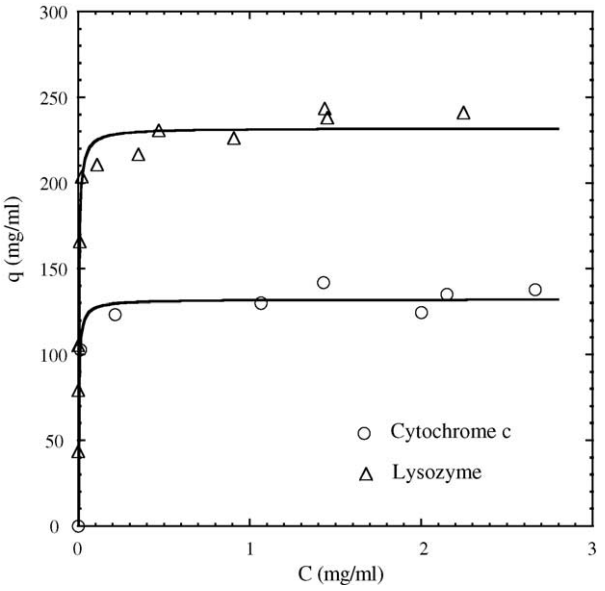

Fig. 10. Adsorption isotherms for lysozyme and cytochrome *c* on SP-Sepharose-FF in 20 mM sodium phosphate buffer at pH 6.5. Lines are Langmuir model fits.

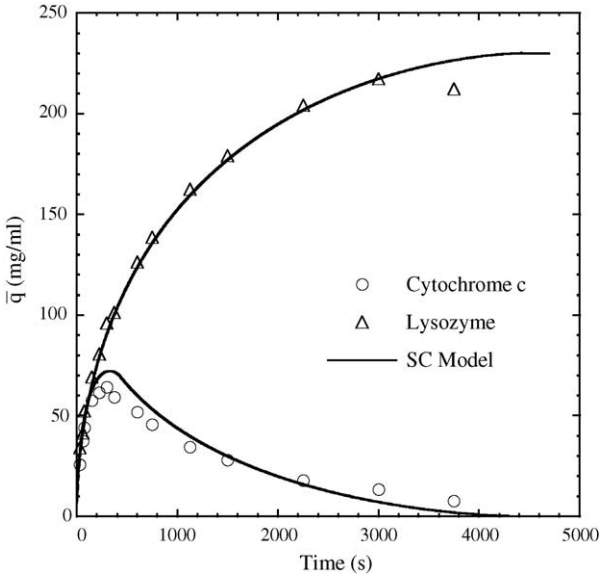

Fig. 12. Two-component simultaneous shallow-bed uptake of a mixture containing 1 mg/ml lyozyme and 1 mg/ml cytochrome *c*. Lines are predictions based on the shrinking core model with $k_f = 0.005$ cm/s.

those based on the analytical irreversible isotherm limit were practically indistinguishable. Interestingly, adsorption of cytochrome *c* occurs at a substantially greater rate than adsorption of lysozyme in spite of the fact that these proteins have similar size and solution diffusivities. Similar results were obtained in shallow-bed experiments with the cytochrome *c* uptake rate being several times faster than the rate for lysozyme.

The results of simultaneous adsorption are shown in Figs. 12 and 13 for shallow-bed and stirred batch experiments with different ratios of protein concentration in solution. In all three cases, cytochrome *c* presents an overshoot in the amount adsorbed before gradually returning to the final equilibrium amount. The latter was essentially zero. In other words, at equilibrium with cytochrome *c* and lysozyme mixture, there was no significant cytochrome *c* adsorption. As seen in Fig. 13, a larger initial concentration of cytochrome *c* in solution results in a greater overshoot. In all cases, however, the return to equilibrium of cytochrome *c* (essentially no adsorption) occurs more slowly at a rate directly proportional to the rate of adsorption of lysozyme.

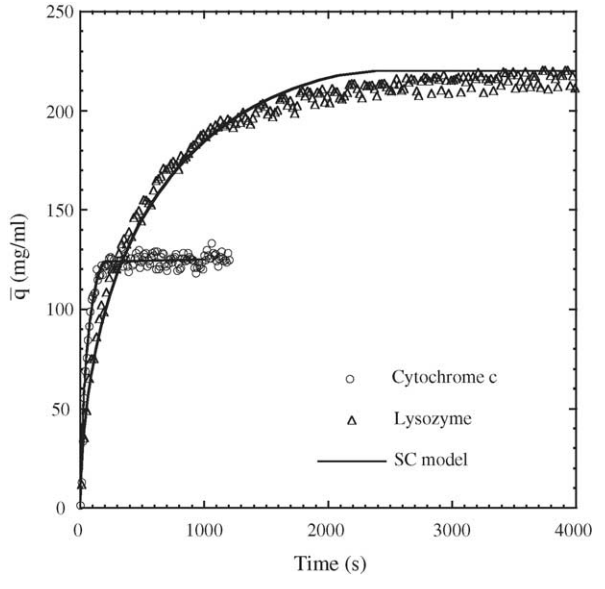

Fig. 11. Single component batch uptake of 2 mg/ml lysozyme and cytochrome *c*. Lines are shrinking core model fits with $k_f = 0.003$ cm/s.

Fig. 14 shows the results of sequential adsorption. In this case, the resin was first saturated with cytochrome *c* and then exposed to a cytochrome *c*/lysozyme mixture. For these conditions, lysozyme completely displaced the adsorbed cytochrome *c* and the rate at which cytochrome *c* is desorbed is consistent with the rate at which lysozyme is adsorbed. It can be seen that the lysozyme uptake curves are very similar whether or not the resin is clean or pre-saturated with cytochrome *c*, indicating that the presence of this pre-adsorbed protein does not affect diffusion of lysozyme in the particles to a significant extent. Moreover, adsorption of lysozyme appears to be completely diffusion controlled and unhindered by the rate of exchange of the two proteins on the adsorbent surface.

Model calculations based on the analytical solution for the irreversible isotherm case are also shown in Figs. 12–14 in comparison with the experimental data. Our experimental system is clearly described by nearly rectangular isotherms with complete displacement of cytochrome *c* by lysozyme. Thus, this situation is analogous to Case III considered in the theoretical part of this work. The numerical solution of the shrinking core equations developed for the general case of adsorption from a finite bath, described in Appendix B, was

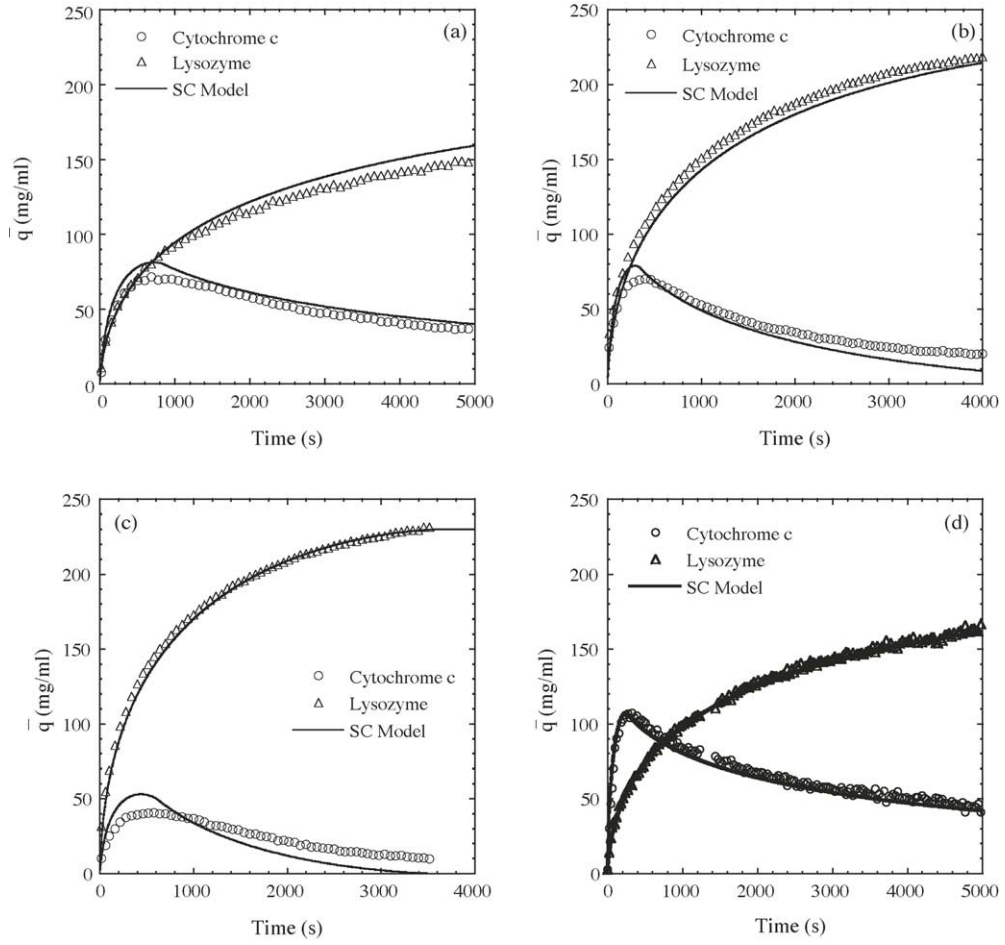

Fig. 13. Two-component simultaneous batch uptake of lyozyme/cytochrome *c* mixtures with different initial concentrations. (a) 0.5/0.5 mg/ml; (b) 1.0/1.0 mg/ml; (c) 1.5/0.5 mg/ml; (d) 0.5/1.5 mg/ml. Lines are predictions based on the shrinking core model with $k_f = 0.003$ cm/s.

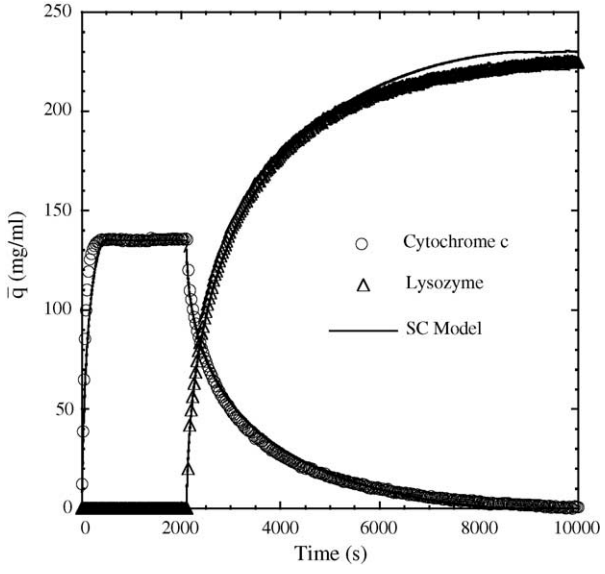

Fig. 14. Two-component sequential batch uptake of 1 mg/ml cytochrome *c* followed by a 1 mg/ml lyozyme/cytochrome *c* mixture. Note that cytochrome *c* is completely displaced by lysozyme. Lines are predictions based on the shrinking core model with $k_f = 0.003$ cm/s.

used for the calculations with the diffusivity values determined form the single component batch uptake experiments using $k_f = 0.003$ cm/s for the batch cases and $k_f = 0.006$ cm/s for the shallow-bed case. In either case, the effect of k_f was almost negligible as for single component adsorption. As seen in these figures, the agreement between experimental and predicted two-component protein adsorption kinetics is quite reasonable. In all cases, the model is in good agreement with the data with regards to the cytochrome *c* overshoot above the equilibrium value and with the slow return to equilibrium. The latter occurs at a rate that is completely controlled by diffusion of lysozyme in the particles. The greatest deviation occurs in Fig. 13c, when there is an excess of lysozyme. For these conditions cytochrome *c* is predicted to form a very thin shell and it is possible that for these conditions more significant deviations from the local equilibrium, rectangular isotherm solution take place. In addition, it is possible that the bound cytochrome *c* could retard to some extent the adsorption rate of lysozyme by introducing an additional kinetic resistance to binding. In any case, this effect seems to be small as shown by the relatively small discrepancy between experimental and predicted results.

5. Conclusions

Predicted intraparticle concentration profiles based on a model for diffusional mass transfer of two proteins in a porous adsorbent suggest the development of concentration patterns with an overshoot of the more weakly adsorbed species above equilibrium followed by a gradual return to equilibrium. The relative magnitude and time of occurrence of the overshoot depends on the relative affinity for the adsorption sites and the diffusivities. An analytical solution can be derived for the rectangular isotherm case. This solution is in good agreement with the general numerical results when the adsorption isotherm is very favorable. For the experimental system considered in this work the two-component adsorption kinetics is consistent with nearly rectangular isotherms and results in complete displacement of one protein by the other. The resulting adsorption patterns are analogous to those predicted by theory. Experimental and predicted batch and shallow-bed adsorption results are in good agreement using a dual-front shrinking core model using diffusivities determined empirically from single component uptake runs.

Acknowledgements

This research was supported by NSF Grant Nos. CTS-0079334 and CTS-0414143. We are all indebted to Professor Csaba Horváth for his incomparable contributions to the field. GC is also especially indebted to Csaba for being an inspiring mentor and a friend who will be dearly missed.

Appendix A

The analytical solution is extended to multicomponent adsorption keeping the assumption that the isotherms are rectangular. For a system with N components ($i = 1, 2, 3, \ldots, N$), where component i completely displaces component $i+1$, the equations to predict the position of the moving fronts with time are developed as follows. For simplicity, we assume that adsorption of the different components is completely mutually exclusive so that each of the adsorption zones that develop in the particle contains a single component. Component 1 is the most strongly adsorbed species and is used as a reference in the ensuing equations.

A.1. Reaction fronts for $t < t_{c_i}$

t_{c_i} is defined as the time at which adsorption front of component i reaches the center of the particle. Up to that time, there are i adsorption fronts moving toward the center of the particle. The advancement of each of these fronts can be described by the following equation

$$2\rho_i^3 - 3\rho_i^2 + 1 = \left(1 + \sum_{k=2}^{i} \beta_{k,1}\right) \frac{t}{\tau_1}, \quad i = 1, 2, \ldots, N \tag{A.1}$$

where $\beta_{k,1} = q_{m,1} D_{e,k} C_k / q_{m,k} D_{e,1} C_1$. t_c is thus given by

$$t_{c_i} = \frac{\tau_1}{1 + \sum_{k=2}^{i} \beta_{k,1}} \tag{A.2}$$

A.2. Reaction fronts for $t \geq t_{c_i}$

In this case, $\rho_i = 0$ so that there are $i-1$ adsorption fronts, with a central core of the particles completely saturated with component i. The equations for the $i-1$ adsorption fronts are the same as Eq. (A.1). Component i is continually desorbed until $\rho_{i+1} = 0$.

Appendix B

The analytical solution for two component adsorption with rectangular isotherms is extended to the case of a finite bath and considering the external mass transfer resistance as follows. For simplicity we consider only the case where component B is completely displaced by A (i.e. $q_B^* = 0$). As before, adsorption occurs in two regimes.

B.1. Reaction fronts for $t < t_c$

In this case, in the outermost layer ($r_A < r < r_p$), the flux of both components is expressed by the same equations as before. Only the boundary conditions are different in order to account for the external mass transfer resistance:

$$r^2 D_{e,A} \frac{dc_A}{dr} = k_A \tag{B.1}$$

$$r^2 D_{e,B} \frac{dc_B}{dr} = k_B \tag{B.2}$$

$$r = r_p: \quad c_A = C_A^s, \qquad c_B = C_B^s \tag{B.3a}$$

$$r = r_A: \quad c_A = 0, \qquad c_B = c_B' \tag{B.3b}$$

Integrating Eqs. (B.1) and (B.2) we obtain:

$$k_A = \frac{D_{e,A} C_A^s}{(1/r_A) - (1/r_p)} \tag{B.4}$$

$$k_B = \frac{D_{e,B}(C_B^s - c_B')}{(1/r_A) - (1/r_p)} \tag{B.5}$$

The advancement of the A adsorption front is obtained from the balance equation:

$$q_{m,A} r_A^2 \frac{dr_A}{dt} = \frac{D_{e,A} C_A^s}{(1/r_p) - (1/r_A)} \tag{B.6}$$

$$t = 0: \quad r_A = r_p \tag{B.7}$$

Introducing dimensionless variables Eq. (B.6) becomes:

$$\frac{d\rho_A}{dt} = \frac{1}{6\tau_A} \frac{C_A^s / C_A^0}{\rho_A(\rho_A - 1)} \tag{B.8}$$

where $\tau = q_{m,A} r_p^2 / 6 D_{e,A} C_A^0$. The ratio of surface and initial solution concentrations, C_A^s / C_A^0, is obtained by combining Eq. (B.8) with the following material balance at the particle surface:

$$\frac{D_{e,A} C_A^s}{(1/\rho_A) - 1} = r_p k_{f,A} (C_A - C_A^s) \tag{B.9}$$

and with the following overall material balance:

$$C_A = C_A^0 [1 - \Lambda_A (1 - \rho_A^3)] \tag{B.10}$$

yielding the result:

$$\frac{d\rho_A}{dt} = \frac{1}{6\tau_A} \frac{1}{\rho_A} \frac{[1 - \Lambda_A (1 - \rho_A^3)]}{(1 - \rho_A) + \rho_A / \mathrm{Bi}_A} \tag{B.11}$$

$$t = 0; \quad \rho_A = 1 \tag{B.12}$$

where $\mathrm{Bi}_A = k_{f,A} r_p / D_{e,A}$ and $\Lambda_A = q_{m,A} V_M / C_A^0 V$.

In the middle layer ($r_B < r < r_A$), the flux of component B is given by:

$$k'_B = \frac{D_{e,B} c'_B r_p}{(1/\rho_B) - (1/\rho_A)} \tag{B.13}$$

while the advancement of the adsorption front for B is obtained from the balance:

$$q_{m,B} \rho_B^2 \frac{d\rho_B}{dt} = \frac{D_{e,B} c'_B}{r_p^2 [(1/\rho_A) - (1/\rho_B)]} \tag{B.14}$$

or

$$\rho_B^2 \frac{d\rho_B}{dt} = \frac{\beta}{6\tau_A} \frac{c'_B / C_B}{(1/\rho_A) - (1/\rho_B)} \tag{B.15}$$

where $\beta = q_{m,A} D_{e,B} C_B^0 / q_{m,B} D_{e,A} C_A^0$. The ratio c'_B / C_B^0 is obtained by combining the following material balance at the A adsorption front:

$$\frac{q_{m,B}}{q_{m,A}} \frac{D_{e,A} C_A^s}{(1/\rho_A) - 1} = \frac{D_{e,B} c'_B}{(1/\rho_B) - (1/\rho_A)} + \frac{D_{e,B} (c'_B - C_B^s)}{(1/\rho_A) - 1} \tag{B.16}$$

with the following material balance at the particle surface:

$$\frac{C_B^s - c'_B}{(1/\rho_A) - 1} = \mathrm{Bi}_B (C_B - C_B^s) \tag{B.17}$$

and with the following overall material balance:

$$C_B = C_B^0 [1 - \Lambda_B (\rho_A^3 - \rho_B^3)] \tag{B.18}$$

where $\Lambda_B = q_{m,B} V_M / C_B^0 V$. The final result is:

$$\frac{c'_B}{C_B^0} = \frac{(\rho_A/\beta)[1 - \Lambda_A (1 - \rho_A^3)] / (1 - \rho_A + \rho_A / \mathrm{Bi}_A) + \rho_A [1 - \Lambda_B (\rho_A^3 - \rho_B^3)] / (1 - \rho_A + \rho_A / \mathrm{Bi}_B)}{1/[(1/\rho_B) - (1/\rho_A)] + 1/[(1/\rho_A) - 1] - [\rho_A^2 / (1 - \rho_A)](1/\mathrm{Bi}_B) / (1 - \rho_A + \rho_A / \mathrm{Bi}_B)} \tag{B.19}$$

and

$$\rho_B^2 \frac{d\rho_B}{dt} = \frac{\beta}{6\tau_A} \frac{(\rho_A/\beta)(1 - \rho_A)[1 - \Lambda_A (1 - \rho_A^3)] / (1 - \rho_A + \rho_A / \mathrm{Bi}_A) + \rho_A (1 - \rho_A)[1 - \Lambda_B (\rho_A^3 - \rho_B^3)] / (1 - \rho_A + \rho_A / \mathrm{Bi}_B)}{-(1 - \rho_A) + \rho_A [(1/\rho_A) - (1/\rho_B)] - [(1/\rho_A) - (1/\rho_B)](\rho_A^2 / \mathrm{Bi}_B) / (1 - \rho_A + \rho_A / \mathrm{Bi}_B)} \tag{B.20}$$

$$t = 0: \quad \rho_B = 1 \tag{B.21}$$

Eqs. (B.11) and (B.20) can be integrated numerically in order to obtain the intraparticle profiles of both components.

B.2. Reaction fronts for $t \geq t_c$

As indicated previously, in this case $\rho_B = 0$; that is, the core of the particle is completely saturated with B and only the A-adsorption front moves toward the center of the particle according to Eq. (B.11). Simultaneously, B is continually desorbed until $\rho_A = 0$.

References

[1] G.L. Skidmore, H.A. Chase, J. Chromatogr. 505 (1990) 329.
[2] W.F. Weinbrenner, M.R. Etzel, J. Chromatogr. A 662 (1994) 414.
[3] R.K. Lewus, G. Carta, AIChE J. 45 (1999) 512.
[4] R.K. Lewus, G. Carta, J. Chromatogr. A 865 (1999) 155.
[5] R.K. Lewus, G. Carta, Ind. Eng. Chem. Res. 40 (2001) 1548.
[6] S.M. Russell, E.B. Belcher, G. Carta, AIChE J. 49 (2003) 1168.
[7] S.M. Russell, G. Carta, AIChE J., 2004, in press.
[8] A. Ljunglof, R. Hjorth, J. Chromatogr. A 743 (1996) 75.
[9] T. Linden, A. Ljunglof, L. Hagel, M.-R. Kula, J. Thommes, Sep. Sci. Technol. 37 (2002) 1.
[10] J. Hubbuch, T. Linden, E. Knieps, J. Thommes, M.-R. Kula, Biotechnol. Bioeng. 80 (2002) 359.
[11] S.R. Dziennik, E.B. Belcher, G.A. Barker, M.J. DeBergalis, S.E. Fernandez, A.M. Lenhoff, Proc. Natl. Acad. Sci. 100 (2003) 421.
[12] L. Hagel, M. Östberg, T. Andersson, J. Chromatogr. A 743 (1996) 33.
[13] J. Hubbuch, T. Linden, E. Knieps, A. Ljunglof, J. Thommes, M.-R. Kula, J. Chromatogr. A 1021 (2003) 93.
[14] S.R. Gallant, J. Chromatogr. A 1028 (2004) 189.
[15] C.A. Brooks, S.M. Cramer, AIChE J. 38 (1992) 1969.
[16] E. Arevalo, M. Rendueles, A. Fernandez, A. Rodrigues, M. Diaz, Sep. Sci. Technol. 13 (1998) 37.
[17] D.M. Ruthven, Principles of Adsorption and Adsorption Processes, Wiley, New York, 1984.
[18] G. Carta, A. Ubiera, AIChE J. 49 (2003) 3066.
[19] A.K. Hunter, G. Carta, J. Chromatogr. A 897 (2000) 81.
[20] G.F. Bloomingburg, J.S. Bauer, G.G. Carta, C.H. Byers, Ind. Eng. Chem. Res. 29 (1991) 1061.